MNRAS **456,** 2095–2104 (2016) doi:10.1093/mnras/stv2777

Unbiased methods for removing systematics from galaxy clustering measurements

Franz Elsner,[1]★ Boris Leistedt[1,2] and Hiranya V. Peiris[1]

[1]*Department of Physics and Astronomy, University College London, London WC1E 6BT, UK*
[2]*Center for Cosmology and Particle Physics, Department of Physics, New York University, New York, NY 10003, USA*

Accepted 2015 November 23. Received 2015 November 23; in original form 2015 September 29

ABSTRACT

Measuring the angular clustering of galaxies as a function of redshift is a powerful method for extracting information from the three-dimensional galaxy distribution. The precision of such measurements will dramatically increase with ongoing and future wide-field galaxy surveys. However, these are also increasingly sensitive to observational and astrophysical contaminants. Here, we study the statistical properties of three methods proposed for controlling such systematics – template subtraction, basic mode projection, and extended mode projection – all of which make use of externally supplied template maps, designed to characterize and capture the spatial variations of potential systematic effects. Based on a detailed mathematical analysis, and in agreement with simulations, we find that the template subtraction method in its original formulation returns biased estimates of the galaxy angular clustering. We derive closed-form expressions that should be used to correct results for this shortcoming. Turning to the basic mode projection algorithm, we prove it to be free of any bias, whereas we conclude that results computed with extended mode projection are biased. Within a simplified setup, we derive analytical expressions for the bias and discuss the options for correcting it in more realistic configurations. Common to all three methods is an increased estimator variance induced by the cleaning process, albeit at different levels. These results enable unbiased high-precision clustering measurements in the presence of spatially varying systematics, an essential step towards realizing the full potential of current and planned galaxy surveys.

Key words: methods: data analysis – methods: numerical – methods: statistical – cosmology: observations – large-scale structure of Universe.

1 INTRODUCTION

Over the last decades, cosmological galaxy surveys collecting statistically representative samples of galaxies over a wide sky area have been become legion (e.g. Huchra et al. 1983; Condon et al. 1998; York et al. 2000; Jones et al. 2004; Cole et al. 2005; Drinkwater et al. 2006; Ilbert et al. 2006; Skrutskie et al. 2006; Kaiser et al. 2010; LSST Dark Energy Science Collaboration 2012; de Jong et al. 2013; Frieman & Dark Energy Survey Collaboration 2013; McMahon et al. 2013; Benítez et al. 2015). An important method for extracting and characterizing galaxy clustering information is the computation of the two-point correlation function on the sphere, the angular correlation function (or its Fourier transform, the angular power spectrum). It has proved invaluable as a powerful interface to confront theoretical cosmological models with observational data (e.g. Totsuji & Kihara 1969; Peebles & Hauser 1974; Hermit et al. 1996; Blake & Wall 2002; Zehavi et al. 2002; Tegmark et al. 2004; Eisenstein et al. 2005; Padmanabhan et al. 2007; Percival et al. 2010; Reid et al. 2010; Beutler et al. 2011; Wake et al. 2011; Busca et al. 2013; Crocce et al. 2015).

With decreasing statistical error bars that result from a steady increase in volume probed by current and future surveys, a proper control of systematic effects, capable of introducing spurious signals, is becoming more and more challenging. Among others, contaminants may be the result of inherent survey characteristics (e.g. survey depth, seeing, or airmass), the details of data gathering and processing (e.g. imprinted by the image calibration procedure), or astrophysical foregrounds (e.g. dust extinction), most of which are spatially varying over the survey footprint. As a result, comprehensive template libraries of maps describing the variation of survey properties over the sky have become a standard data product in state-of-the-art galaxy surveys (Ross et al. 2011, 2012; Leistedt & Peiris 2014; Leistedt et al. 2015). The maps can then be used in a science analysis to either verify the robustness of results, or to actively correct for the impact of systematics.

Several methods have been proposed in literature to use systematics templates to study or reduce the contamination of galaxy

★E-mail: f.elsner@ucl.ac.uk

angular clustering measurements by signals of non-cosmological origin (e.g. Scranton et al. 2002; Blake et al. 2010; Vargas-Magaña et al. 2014, see also Huterer, Cunha & Fang 2013; Morrison & Hildebrandt 2015). In the template subtraction approach introduced in Ho et al. (2012) (also applied in Ross et al. 2011), the level of cross-correlation between systematic template maps and data is used to clean angular clustering estimates of contaminants. An alternative technique, basic mode projection, excludes specific spatial patterns described through a set of templates by assigning infinite variance to them (Rybicki & Press 1992; with applications in, e.g. Tegmark et al. 1998; Slosar, Seljak & Makarov 2004; Smith, Senatore & Zaldarriaga 2009; Elsner & Wandelt 2013; Leistedt et al. 2013). A variant thereof, extended mode projection, was subsequently introduced to identify the most important of all available templates prior to the analysis, to reduce the total number of modes that have to be marginalized over (Leistedt & Peiris 2014; Leistedt, Peiris & Roth 2014).

While many of the proposed methods seem adequate in reducing the impact of systematics, some of them were realized to have a detrimental effect on the galaxy clustering signal (see e.g. the discussion in the appendix of Ross et al. 2012). In this paper, we concentrate on the three systematics mitigation methods mentioned above and study if and in what way the cleaning procedure affects the statistical properties of angular clustering estimates. In particular, we investigate whether the results represent unbiased estimates of the signal properties, and assess if the application of cleaning procedures introduces additional variance to the measurement.

The paper is organized as follows. In Section 2, we provide a detailed discussion of the statistical properties of power spectrum estimates cleaned using the template subtraction method. We then turn our focus to basic and extended mode projection in Section 3, and contrast results obtained in harmonic space and real space (Section 4). Finally, we summarize our findings in Section 5.

2 TEMPLATE SUBTRACTION

In this section, we discuss the properties of a method proposed by Ho et al. (2012) to account for systematic effects that may induce spurious signals. The general idea behind this approach is to use a set of externally supplied templates to be subtracted from the data with optimally chosen weights, which in turn are estimated from a cross-correlation of the template and data. In favour of a transparent discussion, we will first restrict ourselves to the cleaning of a full-sky data set with a single template here and later generalize our results to multiple templates on the cut sky (Section 2.2 and Appendix A).

2.1 Analytical bias calculation, full sky

We first analyse the statistical properties of the proposed estimator. For a single contaminant that contributes to the observed signal with unknown amplitude ϵ, we can construct a linear data model as a first order Taylor expansion in the template f,

$$d = s + \epsilon f, \tag{1}$$

where s is the signal to be inferred from the data vector d of the experiment. It is further assumed that signal and template are uncorrelated, i.e. their cross-covariance vanishes.

Implicitly assuming a non-vanishing template power spectrum $C_\ell^{f\times f}$, in Ho et al. (2012), the authors derive an estimator for the template cleaned signal power spectrum $C_\ell^{s\times s}$,

$$\widehat{C}_\ell^{\mathrm{TS}} = \widehat{C}_\ell^{d\times d} - \hat{\epsilon}^2 \widehat{C}_\ell^{f\times f}, \tag{2}$$

where

$$\hat{\epsilon} = \widehat{C}_\ell^{d\times f} / \widehat{C}_\ell^{f\times f}. \tag{3}$$

For consistency with the proposed method in its original formulation, we consider $\hat{\epsilon}$ to be a function of the multipole moment ℓ in what follows. We hence obtain

$$\begin{aligned}\widehat{C}_\ell^{\mathrm{TS}} &= \widehat{C}_\ell^{d\times d} - \left(\frac{\widehat{C}_\ell^{d\times f}}{\widehat{C}_\ell^{f\times f}}\right)^2 \widehat{C}_\ell^{f\times f} \\ &= \widehat{C}_\ell^{s\times s} - \frac{\left(\widehat{C}_\ell^{s\times f}\right)^2}{\widehat{C}_\ell^{f\times f}}.\end{aligned} \tag{4}$$

It is then possible to check if the estimator is unbiased by calculating the ensemble average of all signal realizations,

$$\left\langle \widehat{C}_\ell^{\mathrm{TS}} \right\rangle = C_\ell^{s\times s} - \frac{1}{C_\ell^{f\times f}} \left\langle \left(\widehat{C}_\ell^{s\times f}\right)^2 \right\rangle. \tag{5}$$

While it may be reasonable to assume that chance correlations between signal and template vanish on average, the same is not true for the square of this product,

$$\begin{aligned}\left\langle \left(\widehat{C}_\ell^{s\times f}\right)^2 \right\rangle &= \left\langle \frac{1}{2\ell+1} \sum_m a_{\ell m}^s a_{\ell m}^{f\,*} \frac{1}{2\ell+1} \sum_{m'} a_{\ell m'}^s a_{\ell m'}^{f\,*} \right\rangle \\ &= \frac{1}{2\ell+1} C_\ell^{s\times s} C_\ell^{f\times f},\end{aligned} \tag{6}$$

where we made use of the statistical isotropy of the signal, $\left\langle a_{\ell m}^s a_{\ell m'}^{s\,*} \right\rangle = C_\ell^{s\times s} \delta_{mm'}$. We therefore obtain for the ensemble average

$$\left\langle \widehat{C}_\ell^{\mathrm{TS}} \right\rangle = C_\ell^{s\times s} \left(1 - \frac{1}{2\ell+1}\right), \tag{7}$$

i.e., the estimator is biased low, with a relative bias of $b_\ell = -1/(2\ell+1)$. It can be shown (see Appendix A1) that the bias scales with the number of independent templates used in the cleaning process,

$$b_\ell = -n/(2\ell+1). \tag{8}$$

2.2 Analytical bias calculation, cut sky

Finally, we extend our full-sky results obtained so far to the more realistic case where data are available only on a fraction of the sphere. In the following, we will assume that all power spectra have been calculated with a pseudo-C_ℓ power spectrum estimation code (Hivon et al. 2002) which allows us to develop our results self-consistently within a common framework. We note, however, that the use of other (e.g. maximum likelihood) estimators is possible but leaves our conclusions unchanged.

On the cut sky, the spherical harmonics lose their orthogonality, which manifests itself in a coupling between formerly uncorrelated Fourier modes. Here, we have to modify equation (6) to take this effect into account. Making use of the properties of the coupling kernels, we obtain for the ensemble averaged, mask deconvolved

signal power spectrum

$$\left\langle \left(\widehat{C}_\ell^{s\times f}\right)^2 \right\rangle = \left\langle \sum_{\ell_1} M^{-1}_{\ell\ell_1} \frac{1}{2\ell_1+1} \sum_{m_1} a^s_{\ell_1 m_1} a^{f\,*}_{\ell_1 m_1} \times \sum_{\ell_2} M^{-1}_{\ell\ell_2} \frac{1}{2\ell_2+1} \sum_{m_2} a^s_{\ell_2 m_2} a^{f\,*}_{\ell_2 m_2} \right\rangle = \sum_{\ell_1\ell_2\ell_3} \left(M^{-1}_{\ell\ell_1}\right)^2 \frac{1}{2\ell_1+1} M_{\ell_1\ell_2} M_{\ell_1\ell_3} C^{s\times s}_{\ell_2} C^{f\times f}_{\ell_3}, \quad (9)$$

where $M_{\ell\ell'}$ are the coupling matrices (see Appendix A2 for formal definitions and details of the calculation). On the cut sky, equation (7) hence takes the more complicated form

$$\left\langle \widehat{C}_\ell^{\rm TS} \right\rangle = C_\ell^{s\times s} \times \left(1 - \frac{\sum_{\ell_1\ell_2\ell_3} \left(M^{-1}_{\ell\ell_1}\right)^2 \frac{1}{2\ell_1+1} M_{\ell_1\ell_2} M_{\ell_1\ell_3} C^{s\times s}_{\ell_2} C^{f\times f}_{\ell_3}}{C_\ell^{s\times s} C_\ell^{f\times f}} \right), \quad (10)$$

which correctly reduces to equation (7) in the full-sky limit. We can then just read off the multipole-dependent relative bias,

$$b_\ell = - \frac{\sum_{\ell_1\ell_2\ell_3} \left(M^{-1}_{\ell\ell_1}\right)^2 \frac{1}{2\ell_1+1} M_{\ell_1\ell_2} M_{\ell_1\ell_3} C^{s\times s}_{\ell_2} C^{f\times f}_{\ell_3}}{C_\ell^{s\times s} C_\ell^{f\times f}}. \quad (11)$$

Lastly, we discuss the most general case considered here, the cleaning of a data set on the cut sky with multiple templates. Building on the results derived in Appendix A1, the relative bias is

$$b_\ell = -\frac{1}{C_\ell^{s\times s}} \left\langle \widehat{\boldsymbol{C}}_\ell^{s\times f\,\dagger} \widehat{\boldsymbol{C}}_\ell^{f\times f\,-1} \widehat{\boldsymbol{C}}_\ell^{s\times f} \right\rangle = -\frac{1}{C_\ell^{s\times s}} \sum_{ij} \left(\boldsymbol{C}_\ell^{f\times f\,-1} \right)_{ij} \times \sum_{\ell_1\ell_2\ell_3} \left(M^{-1}_{\ell\ell_1}\right)^2 \frac{1}{2\ell_1+1} M_{\ell_1\ell_2} M_{\ell_1\ell_3} C^{s\times s}_{\ell_2} C^{f_i\times f_j}_{\ell_3}. \quad (12)$$

We provide an approximate estimate of the bias on the cut sky that reflects the scaling of the coupling matrices with the sky fraction,

$$b_\ell \sim -n / \left(f_{\rm sky}^2 (2\ell+1) \right), \quad (13)$$

where n is the number of independent templates used in the analysis. We stress that the accuracy of equation (13) depends sensitively on the functional form of signal-, template-, and mask power spectra, and is only valid for large to intermediate sky fractions.

2.3 Verification with simulations

We now confirm the results obtained thus far using 1000 simulated Gaussian random maps drawn from a flat power spectrum. To showcase the biasing effect of the cleaning procedure, we generated a set of 10 independent random templates to be subtracted from the simulated maps. After a power spectrum analysis on the full sky using the template subtraction method, equation (2), we computed the relative deviation of the averaged recovered power spectra with respect to the input. The observed multipole-dependent bias, shown in Fig. 1, is in good agreement with the analytical estimate.

We then verified our understanding of the cleaning process on the cut sky. Using an azimuthally symmetric binary mask that restricts the power spectrum measurement to latitudes of $-40^\circ \leq b \leq 40^\circ$ ($f_{\rm sky} \approx 65$ per cent), we analysed 1000 simulations using a pseudo-C_ℓ estimator. After applying the cleaning procedure, we again computed the bias of the result. As can be seen in Fig. 2, it has increased substantially compared to the full-sky analysis. Aside from the exact analytical estimate, we also compare the numerical results to the approximate bias description given in equation (13). We obtain good agreement between simulations and analytical expressions.

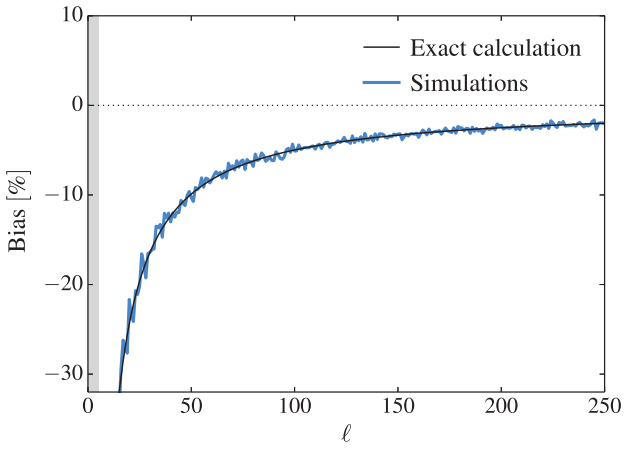

Figure 1. Direct subtraction of systematic templates leads to biased power spectrum estimates. Removing contributions from 10 templates, we show the resulting relative bias of the averaged power spectrum of 1000 simulations (blue solid line) and its analytical prediction (black solid line). In the multipole region where $\ell \leq (n-1)/2$, a cleaned power spectrum cannot be constructed (grey region to the left).

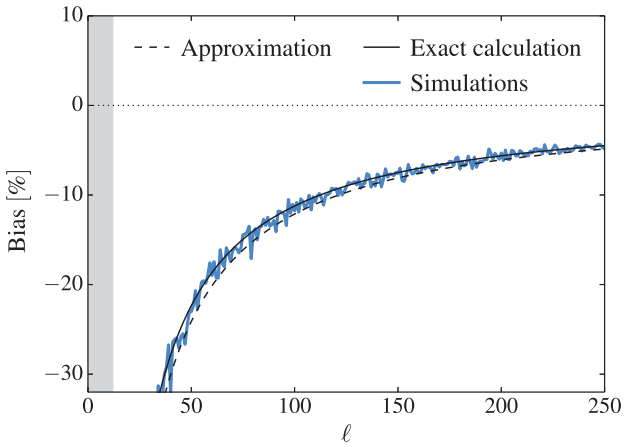

Figure 2. Same as Fig. 1, but for partial sky coverage. The bias becomes larger for a cut-sky analysis. Keeping all other simulation parameters the same, we computed pseudo-C_ℓ power spectra on about 65 per cent of the sky. The approximate analytical bias estimate, obtained from a simple rescaling of the full-sky results, is also shown (black dashed line).

2.4 Discussion

The bias identified in the previous paragraphs can be understood intuitively. Even if signal and template are uncorrelated on average, there will still be chance correlations for every individual signal realization. By construction, the cleaning procedure will then minimize the cross-correlation between signal and template, thereby leading to an overcorrection in the ensemble mean. To be more

precise, since the cleaning coefficients $\hat{\epsilon}$ are computed for all multipole moments individually, at a given ℓ, the power in one of the $(2\ell + 1)$ available Fourier modes will be removed by each template, giving rise to the simple expression in equation (8). From a more formal point of view, the problem arises from the fact that while we derive an estimate of the cleaning coefficient $\hat{\epsilon}$ in equation (3), we use its square (i.e. a non-linear transform of it) in the cleaning step equation (2). Although we indeed obtain $\langle\hat{\epsilon}\rangle = \epsilon$ on average, we however find $\langle\hat{\epsilon}^2\rangle \neq \epsilon^2$.

It is interesting to discuss the limiting case where the number of independent Fourier modes in the data drops below the number of cleaning templates, $(2\ell + 1) < n$ for a full-sky data set. For each of these multipole moments ℓ, the $n \times n$ matrix constructed from all possible template auto- and cross-power spectra becomes rank deficient. As a result, a unique solution for the cleaning coefficients $\hat{\epsilon}$ no longer exists.[1] What is more, and this also includes the case where $2\ell + 1 = n$, the template-subtracted power spectrum estimates $\widehat{C}_\ell^{s\times s}$ vanish by construction and a meaningful conclusion about the cleaned signal amplitude cannot be drawn.

Owing to the aggressive scaling with the sky fraction, $b_\ell \propto f_{\rm sky}^{-2}$, on the cut sky the bias can become substantial even when the data set is cleaned with only a single template. Fortunately, since we derived closed-form expressions for the bias, we can naturally propose a correction procedure: to obtain unbiased power spectrum estimates only requires the multiplication of all $\widehat{C}_\ell^{s\times s}$ estimates with the multipole-dependent factor $1/(1 + b_\ell)$, where b_ℓ is given by one of the expressions in equations (8), (2), or (13). As discussed above, depending on the number of templates used, a correction will not be possible for multipoles below a certain $\ell_{\rm min}$.

It is also worth noting that the cleaning procedure comes at a price. Since the effective number of Fourier modes available to measure $\widehat{C}_\ell^{s\times s}$ is reduced, the final bias-corrected power spectrum estimates will suffer from excess variance (i.e. they have larger error bars). More quantitatively, while a cosmic variance-limited estimate of a power spectrum computed on the full sky has variance $\mathrm{Var}(\widehat{C}_\ell) = 2C_\ell^2/(2\ell + 1)$, the template cleaning process increases the uncertainty in the measurement to $\mathrm{Var}(\widehat{C}_\ell^{s\times s}) = 2(C_\ell^{s\times s})^2/(2\ell + 1 - n)$. The impact of the cleaning process on the error bars of clustering measurements has not been identified and addressed in previous applications of this method.

While the cleaning coefficient $\hat{\epsilon}$ in equation (2) is a function of multipole moment in the original formulation of the algorithm, other authors have assumed it constant within power spectrum bins (e.g. Giannantonio et al. 2015), or decided to keep it fixed entirely (e.g. Ross et al. 2011). Restricting the number of free parameters in the cleaning procedure will then result in a reduced bias, since chance correlations are removed only to a lesser extent. However, these approaches also leave less freedom in case the systematics templates can only approximately capture the signal contamination, and may therefore increase the systematics residuals in the cleaned clustering estimate. Since an analytical calculation of the bias is no longer possible for these variants of the template subtraction method, simulations would be required to correct clustering estimates in practical applications.

Our analytical studies also provide a more principled explanation for the results of numerical tests conducted in Ross et al. (2012) on mock galaxy catalogues to aid the analysis of *BOSS* data. While the authors compare variations of the template subtraction method which only allow for a qualitative comparison, they also find that the cleaning procedure results in a negative bias of galaxy clustering estimates, in agreement with the results presented here.

We note in passing that results obtained in this section resemble the bias identified in so-called internal linear combination (ILC) maps constructed from multifrequency observations of the cosmic microwave background radiation (see the discussion in e.g. Hinshaw et al. 2007; Saha et al. 2008).

[1] Of course, it is still possible to obtain a (non-unique) solution to the system of equations, for example by means of the Moore–Penrose pseudo-inverse.

3 MODE PROJECTION

An alternative method for subtracting a set of templates from a data set was proposed by Rybicki & Press (1992). It can be straightforwardly included into the optimal quadratic power spectrum estimator for which the computation is based on inverse variance weighted combinations of the data vector (Tegmark 1997).

3.1 Basic mode projection

We first discuss the basic mode projection approach marginalising over a single template. The underlying idea of this technique is to modify the signal covariance matrix to assign infinite variance to modes that are to be excluded from the analysis. In the following, we verify the unbiasedness of the derived power spectra.

3.1.1 Analytical bias calculation

Let us first review the basic equations of the optimal quadratic estimator (Tegmark 1997). To simplify the discussion, we will consider a full-sky analysis of noiseless data and choose the spherical harmonic space as basis for our calculations. Retaining the data model defined in equation (1), the estimator derives the power spectrum from a quadratic combination of the data,

$$\widehat{C}_\ell^{s\times s} = \sum_{\ell'} N^{-1}_{\ell\ell'} \boldsymbol{d}^\dagger \boldsymbol{E}_{\ell'} \boldsymbol{d}, \tag{14}$$

where N is the estimator normalization given by the Fisher matrix $N_{\ell\ell'} = 2F_{\ell\ell'}$. Here, the $(\ell_{\rm max} + 1)^2 \times (\ell_{\rm max} + 1)^2$ matrices

$$\boldsymbol{E}_\ell = \boldsymbol{C}^{-1} \frac{\partial \boldsymbol{C}}{\partial C_\ell} \boldsymbol{C}^{-1} \tag{15}$$

are expressed as a function of the covariance matrix

$$\boldsymbol{C} = \sum_\ell C_\ell \boldsymbol{D}_\ell, \tag{16}$$

which takes a particularly simple form since we work in spherical harmonic space. The matrices $\boldsymbol{D}_\ell$ are diagonal and of rank $(2\ell + 1)$,

$$(\boldsymbol{D}_\ell)_{ij} = \begin{cases} \delta_{ij} & \ell^2 < i \leq (\ell+1)^2 \\ 0 & \text{otherwise} \end{cases}, \tag{17}$$

trivially fulfilling the useful relation $\boldsymbol{D}_\ell \boldsymbol{D}_{\ell'} = \boldsymbol{D}_\ell\, \delta_{\ell\ell'}$.

Mode projection is now included by means of a rank-one update to the covariance matrix in the equations above, $\widetilde{\boldsymbol{C}} = \lim_{\sigma\to\infty} \boldsymbol{C} + \sigma f f^\dagger$. The Sherman–Morrison formula allows the inverse to be calculated exactly,

$$\widetilde{\boldsymbol{C}}^{-1} = \boldsymbol{C}^{-1} - \frac{\boldsymbol{C}^{-1} f f^\dagger \boldsymbol{C}^{-1}}{f^\dagger \boldsymbol{C}^{-1} f}. \tag{18}$$

We obtain for the ensemble-averaged, unnormalized signal power spectrum estimate

$$\left\langle \boldsymbol{d}^\dagger \widetilde{\boldsymbol{E}}_\ell \boldsymbol{d} \right\rangle = \frac{2\ell+1}{C_\ell^{s\times s}} \left(1 - \frac{C_\ell^{f\times f}/C_\ell^{s\times s}}{\sum_{\ell'}(2\ell'+1)C_{\ell'}^{f\times f}/C_{\ell'}^{s\times s}} \right), \tag{19}$$

an identity which we derive in Appendix B1. The diagonal elements of the normalization factor, used to calibrate the estimator, are

$$\begin{aligned}\widetilde{N}_{\ell\ell} &= \mathrm{tr}\left(\widetilde{\boldsymbol{C}}^{-1} \frac{\partial \widetilde{\boldsymbol{C}}}{\partial C_\ell} \widetilde{\boldsymbol{C}}^{-1} \frac{\partial \widetilde{\boldsymbol{C}}}{\partial C_\ell} \right) \\ &= \frac{2\ell+1}{\left(C_\ell^{s\times s}\right)^2} \left(1 - \frac{2C_\ell^{f\times f}/C_\ell^{s\times s}}{\sum_{\ell'}(2\ell'+1)C_{\ell'}^{f\times f}/C_{\ell'}^{s\times s}} \right. \\ &\quad \left. + \frac{(2\ell+1)\left(C_\ell^{f\times f}/C_\ell^{s\times s}\right)^2}{\left(\sum_{\ell'}(2\ell'+1)C_{\ell'}^{f\times f}/C_{\ell'}^{s\times s}\right)^2} \right),\end{aligned} \tag{20}$$

as detailed in Appendix B1. Note that although we work on the full sky, once mode projection is included the Fisher matrix is no longer diagonal,

$$\begin{aligned}\widetilde{N}_{\ell\ell'} &= \mathrm{tr}\left(\widetilde{\boldsymbol{C}}^{-1} \frac{\partial \widetilde{\boldsymbol{C}}}{\partial C_\ell} \widetilde{\boldsymbol{C}}^{-1} \frac{\partial \widetilde{\boldsymbol{C}}}{\partial C_{\ell'}} \right) \\ &= \frac{2\ell+1}{C_\ell^{s\times s} C_{\ell'}^{s\times s}} \frac{C_\ell^{f\times f}/C_\ell^{s\times s}(2\ell'+1)C_{\ell'}^{f\times f}/C_{\ell'}^{s\times s}}{\left(\sum_{\ell''}(2\ell''+1)C_{\ell''}^{f\times f}/C_{\ell''}^{s\times s}\right)^2}\end{aligned} \tag{21}$$

for $\ell \neq \ell'$. This newly introduced effect of mode coupling is in agreement with the interpretation that mode projection is in fact equivalent to masking. It is then possible to prove that

$$\begin{aligned}\left\langle \widehat{C}_\ell^{\mathrm{BMP}} \right\rangle &= \sum_{\ell'} \widetilde{N}_{\ell\ell'}^{-1} \left\langle \boldsymbol{d}^\dagger \widetilde{\boldsymbol{E}}_{\ell'} \boldsymbol{d} \right\rangle \\ &= C_\ell^{s\times s}\end{aligned} \tag{22}$$

(see Appendix B2), i.e. the basic mode projection algorithm is unbiased.

3.1.2 *Verification with simulations*

To verify results obtained for the basic mode projection algorithm, we applied the technique to a set of 1000 simulated maps and templates with the same properties as previously introduced in Section 2.3. We used the identical mask ($f_{\mathrm{sky}} \approx 65$ per cent) and restricted the analysis to relatively low resolution to accommodate the comparatively high computational complexity of the optimal quadratic estimator. We show binned measurements of the relative bias computed from the averaged power spectrum in Fig. 3, where we projected out 10 independent templates. In agreement with the theoretical analysis presented above, we find no evidence for a bias in power spectrum measurements with basic mode projection. Comparing the diagonal elements of the Fisher matrix with and without mode projection enabled, we also show the increase in error bars of the power spectrum coefficients induced by the cleaning procedure.

3.1.3 *Discussion*

Unlike the template subtraction approach discussed in Section 2, basic mode projection correctly accounts for the reduced variance in power spectrum estimates in equation (19) with an appropriately

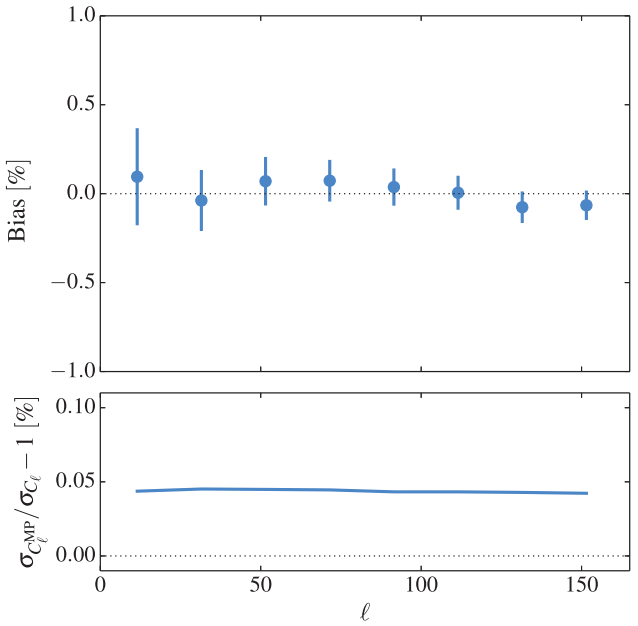

Figure 3. Basic mode projection leads to unbiased power spectrum estimates. Top panel: the average power spectrum estimate of 1000 simulated maps, computed on the cut sky with an optimal quadratic estimator with basic mode projection, is consistent with the input over the full multipole range (blue circles). Bottom panel: the increase in error bars of the power spectrum measurement as a result of mode projection is in the sub-percentage regime.

rescaled expression for the estimator normalization equations (20) and (21). Although we restricted the analytical derivations in this section to the case of a single template, this conclusion seems to hold for arbitrary numbers of templates, as indicated by the results of our numerical studies. Likewise, since the quadratic estimator takes into account the analysis mask in a mathematically exact way, the discussion extends to the cut-sky case.

The inverse of the normalization provides us with direct access to the estimator variance. In contrast to the template subtraction method in Section 2, the more complicated mathematical expressions make a straightforward interpretation difficult. If we assume, however, a constant ratio of template to signal power spectra, we can gain some insights by deriving an approximate expression for the variance of the signal power spectrum estimate. Considering the case of a full-sky data set with mode projection of a single template, we obtain

$$\mathrm{Var}(\widehat{C}_\ell^{s\times s}) \approx \frac{2(C_\ell^{s\times s})^2}{2\ell+1} \left(1 + \frac{1}{(\ell_{\mathrm{max}}+1)^2} \right). \tag{23}$$

Alternatively, we can express the increased variance in terms of a reduced effective sky fraction of the experiment,

$$\mathrm{Var}(\widehat{C}_\ell^{s\times s}) \approx \frac{2(C_\ell^{s\times s})^2}{(2\ell+1)\, f_{\mathrm{sky}}^{\mathrm{eff}}}, \tag{24}$$

where we have defined $f_{\mathrm{sky}}^{\mathrm{eff}} \approx 1 - 1/(\ell_{\mathrm{max}}+1)^2 < 1$. Here, the excess variance is approximately given by the ratio of the single template mode projected to the total number of Fourier modes present in a data set band-limited at ℓ_{max}. We observe a smaller increase in variance compared to the template subtraction method, where the cleaning procedure is applied at every multipole moment independently. Still, some of the discussion in Section 2.4 also applies to mode projection: in case the number of templates is too large

compared to the number of Fourier modes at multipole moment ℓ, power spectrum estimation is rendered impossible.

3.2 Extended mode projection

Although basic mode projection is unbiased, including template marginalization over a large number, possibly thousands, of systematics maps will result in a substantial increase in estimator variance, considerably degrading the predictive power of the data set. This observation prompted the development of the extended mode projection algorithm (Leistedt & Peiris 2014), where a smaller subset of templates to be projected is selected among all available templates by means of some heuristic criterion prior to the power spectrum analysis. The idea behind the selection process is to identify systematic maps that show noticeable correlations with the data and may therefore be adequate tracers of spurious signals. Systematic maps that are not or only slightly correlated with the data, on the other hand, appear to lack relevance for describing possible contaminants and are therefore excluded from being marginalized over.

3.2.1 Analytical bias calculation

In the following, we assess the effects of the template selection step on the statistical properties of the power spectrum estimate. To do so, we first have to specify a selection criterion. While an approximate χ^2 estimate computed from the cross-power spectrum of signal and template was used in the original formulation of the algorithm (Leistedt & Peiris 2014), here we adopt a simplified measure to enable a more transparent discussion. We consider a full-sky experiment and a template f, containing power only at a single multipole moment $f_{\ell m} \propto \delta_{\ell\ell'}\delta_{m0}$. Setting $a_{\ell 0}$ to be the spherical harmonic coefficient of the data vector corresponding to the template mode, we adopt a selection criterion based on a predefined threshold $t \geq 0$ such that the extended mode projection algorithm defaults to a standard power spectrum estimation method if $|a_{\ell 0}| \leq t$, while it otherwise makes use of basic mode projection.

We compute the ensemble average of the signal power spectrum estimate to check if the estimator is unbiased. For this first test, we assume that the data is free of any contaminant. In that case,

$$\begin{aligned}\left\langle \widehat{C}_\ell^{\mathrm{EMP}} \right\rangle = \Bigg\langle & \prod_{m\neq 0} \int_{-\infty}^{\infty} \mathrm{d}a_{\ell m} \int_{-\infty}^{-t} \mathrm{d}a_{\ell 0}\, P(\{a_{\ell m}\}) \frac{\sum_m |a_{\ell m}|^2}{2\ell+1} \\ & + \prod_{m\neq 0} \int_{-\infty}^{\infty} \mathrm{d}a_{\ell m} \int_{-t}^{t} \mathrm{d}a_{\ell 0}\, P(\{a_{\ell m}\}) \frac{\sum_{m\neq 0} |a_{\ell m}|^2}{2\ell} \\ & + \prod_{m\neq 0} \int_{-\infty}^{\infty} \mathrm{d}a_{\ell m} \int_{t}^{\infty} \mathrm{d}a_{\ell 0}\, P(\{a_{\ell m}\}) \frac{\sum_m |a_{\ell m}|^2}{2\ell+1} \Bigg\rangle \\ = C_\ell^{s\times s} & \left(1 - \sqrt{\frac{2}{\pi C_\ell^{s\times s}}} \frac{t}{2\ell+1} \mathrm{e}^{-\frac{t^2}{2C_\ell^{s\times s}}}\right), \end{aligned} \tag{25}$$

for a Gaussian random field $a_{\ell m}$. We conclude that for the case considered here, power spectra estimated with the extended mode projection algorithm are biased with a relative bias of

$$b_\ell = -\sqrt{\frac{2}{\pi C_\ell^{s\times s}}} \frac{t}{2\ell+1} \mathrm{e}^{-\frac{t^2}{2C_\ell^{s\times s}}}. \tag{26}$$

In the presence of a contaminating signal that can be perfectly characterized by the template, however, the situation changes. For the updated data model $d = s + kf$, where $k = \epsilon/\sqrt{C_\ell^{s\times s}} \geq 0$ is the relative level of contamination, the integral bounds in equation (25) shift from $\pm t$ to $\pm t - k$. We then obtain a generalized form of equation (26),

$$\begin{aligned} b_\ell = & -\sqrt{\frac{2}{\pi C_\ell^{s\times s}}} \frac{1}{2(2\ell+1)} \left(t - k + (t+k)\,\mathrm{e}^{\frac{2tk}{C_\ell^{s\times s}}}\right) \mathrm{e}^{-\frac{(t+k)^2}{2C_\ell^{s\times s}}} \\ & - \frac{k^2}{2(2\ell+1)C_\ell^{s\times s}} \left[\mathrm{erf}\left(\frac{k-t}{\sqrt{2C_\ell^{s\times s}}}\right) - \mathrm{erf}\left(\frac{k+t}{\sqrt{2C_\ell^{s\times s}}}\right)\right], \end{aligned} \tag{27}$$

where the bias becomes a function of the additional parameter k. We note that the results obtained in equations (26) and (27) are only valid for the selection criterion introduced above.

3.2.2 Verification with simulations

To test our results for correctness, we again compare the analytical results derived in the previous paragraph to simulations. Since equations (26) and (27) are both functions of the selection threshold t, we present results of the parameter exploration for a fixed multipole moment, $\ell = 5$. To verify the first case discussed, equation (26), we simulate 100 000 systematics-free data sets. We compute power spectra using extended mode projection with a single template, where we chose the values of the threshold parameter from a regularly spaced grid. To check the second result, equation (27), we prepared a new set of simulations, adding a constant contribution of a contaminant with amplitude $k = 0.5$. In Fig. 4, the derived relative bias estimates are plotted as a function of the selection threshold. Comparing the analytical formula to simulation results, we find good agreement.

3.2.3 Discussion

Although the extended mode projection algorithm is a very close derivative of basic mode projection, the two approaches to systematics mitigation behave qualitatively differently regarding their ensemble averaged power spectrum estimates. For extended mode projection, we find in general a non-zero bias whose exact numerical value is dependent on the template selection criterion adopted in the analysis. In agreement with results presented in Section 3.1, the bias vanishes in the limit $t \to 0$, where extended mode projection becomes equivalent to basic mode projection. Likewise, if the data are free of systematics, the bias goes to zero in the limit $t \to \infty$, where extended mode projection reduces to simple power spectrum estimation. The latter result changes, however, in case there is a contaminant contributing to the observed signal. If it can be captured by the template, then there exists a non-zero value of the threshold parameter for which the power spectrum estimates become unbiased. Unfortunately, to locate this sweet spot would require knowledge of the actual level of systematics in the data, which will not be easily available in real-world applications. Although beyond the scope of this paper, we note that forward-modelling simulations, attempting to model the full transfer function of the survey including systematic effects, appear to be well-suited to provide the additional information needed to debias signal power spectra (Bergé et al. 2013; Busha et al. 2013; Chang et al. 2015).

It is relatively straightforward to identify the source of the observed bias. Since the template selection process is based on the actual data realization, it will inevitably be influenced by chance correlations between signal and template. As a result, for the selection criterion adopted here, larger values of the signal amplitude are

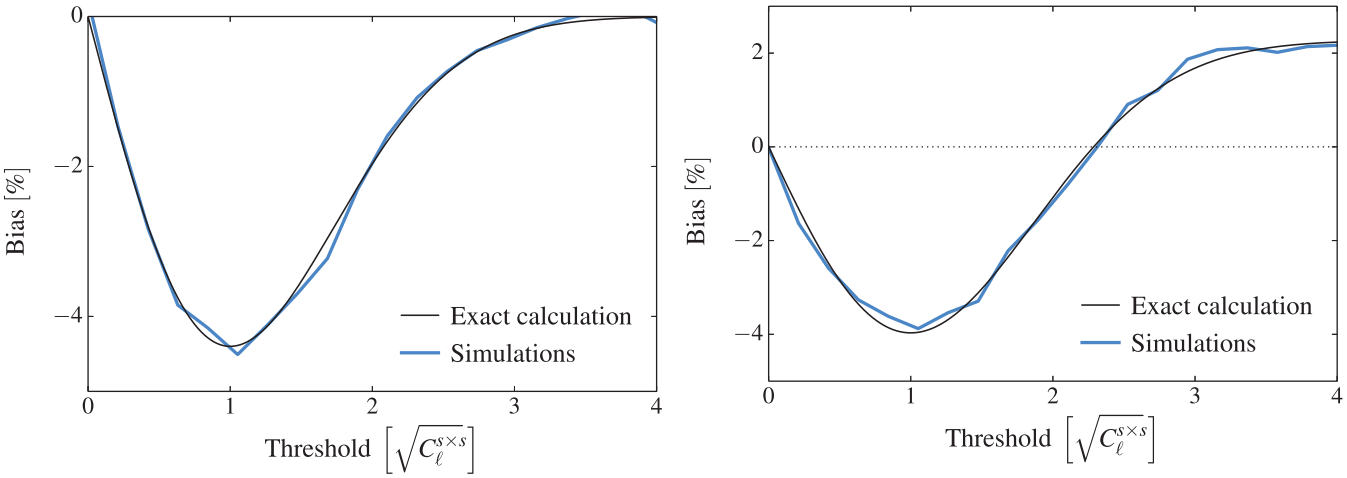

Figure 4. Extended mode projection power spectrum estimates can be biased. For a single template analysis, we show the relative bias of the algorithm as a function of the template selection threshold from simulations (blue solid lines) and analytical estimates (black solid lines) for the multipole moment $\ell = 5$. The bias is strictly non-positive in case the data are intrinsically free of any contaminants (left-hand panel), while it otherwise crosses zero (right-hand panel).

more likely to trigger the use of mode projection than smaller values, leading to an underestimation of the signal variance on average.

4 RESULTS FOR ANGULAR CORRELATION FUNCTION MEASUREMENTS

Since we assumed an isotropic signal, results in the previous sections have been exclusively derived in spherical harmonic space, a basis where symmetries simplify most of the analytical calculations considerably. Real space angular correlation functions are widely used in the field of large-scale structure analysis. Their information content is equivalent; they are related to power spectrum measurements in a mathematically exact way,

$$w(\theta) = \sum_{\ell=0}^{\infty} \frac{2\ell+1}{4\pi} C_\ell P_\ell\left(\cos(\theta)\right), \tag{28}$$

where the P_ℓ are Legendre polynomials of degree ℓ.

In the following, we discuss the generalization of our harmonic space results to real space. Unfortunately, since the most popular angular correlation function estimator introduced by Landy & Szalay (1993) does not use the inverse variance weighted data vector as basis for the calculation, the mode projection methods reviewed in Section 3 cannot be straightforwardly extended to real space analyses applying this estimator. We will therefore only consider the template subtraction method of Section 2.

4.1 Analytical bias calculation

To obtain real-space expressions for the bias, we first discuss the direct transformation of our results from Section 2 to real space, i.e. still assuming that the cleaning procedure itself was performed in harmonic space. Given an analytical expression for the multipole-dependent relative bias b_ℓ of the signal power spectrum, we obtain for the ensemble averaged angular correlation function

$$\begin{aligned}\left\langle \widehat{w}(\theta)^{\mathrm{TS}} \right\rangle &= w^{s\times s}(\theta) + \sum_{\ell=0}^{\infty} \frac{2\ell+1}{4\pi} \left(b_\ell\, C_\ell^{s\times s}\right) P_\ell\left(cos(\theta)\right) \\ &= w^{s\times s}(\theta) + w^b(\theta),\end{aligned} \tag{29}$$

where the real-space bias term $w^b(\theta)$ now always implicitly depends on $C_\ell^{s\times s}$ and cannot be easily expressed as a multiplicative correction to $w^{s\times s}(\theta)$. This is a characteristic property, typical for the mixing of Fourier modes in angular correlation function measurements. Given the bias derived in harmonic space, equation (12) (or its approximation, equation 13), it is then possible to obtain equivalent real space expressions to debias angular correlation function measurements cleaned with the template subtraction method using equation (29).

In the more realistic case where the full analysis, including the cleaning step, is performed in real space, the situation grows more complex. Building on the formalism developed for the harmonic space analysis in Section 2 and Appendix A, we find for angular correlation function estimates on the cut sky, cleaned with multiple templates,

$$\begin{aligned}\left\langle \widehat{w}(\theta)^{\mathrm{TS}} \right\rangle &= w^{s\times s}(\theta) - \left\langle \widehat{\boldsymbol{w}}(\theta)^{s\times f\,\dagger} \widehat{\boldsymbol{w}}(\theta)^{f\times f\,-1} \widehat{\boldsymbol{w}}(\theta)^{s\times f} \right\rangle \\ &= w^{s\times s}(\theta) - \sum_{ij} \left(\boldsymbol{w}(\theta)^{f\times f\,-1}\right)_{ij} w^{s s\times f_i f_j}(\theta),\end{aligned} \tag{30}$$

where we identify the second term on the right-hand side as bias $w^b(\theta)$. If the analysis is performed on the full sky, for example, we find

$$w^{s s\times f_i f_j}(\theta) = \sum_\ell \left(\frac{2\ell+1}{4\pi} P_\ell\left(cos(\theta)\right)\right)^2 \frac{1}{2\ell+1} C_\ell^{s\times s} C_\ell^{f_i\times f_j}. \tag{31}$$

To derive this expression for the bias in real space, we again needed to make use of the isotropy of the signal in the Fourier domain. As before, the mode mixing in angular correlation function estimates prevents us from writing the estimator bias term in equation (31) as a signal-independent multiplicative factor.

4.2 Verification with simulations

To demonstrate the correctness of our calculation, we computed angular correlation function estimates of 1000 simulated maps, cleaned with the template subtraction method in real space. To this end, we generated band-limited Gaussian maps drawn from a $C_\ell \propto (\ell+1)^{-1}$ power spectrum, smoothly truncated at ℓ_{max} using a cosine apodization. We derived correlation function measurements of the signal on the full sky using 10 templates in the cleaning

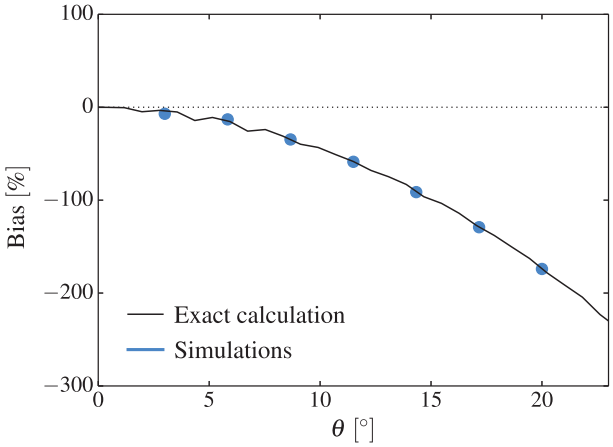

Figure 5. Same as Fig. 1, but for measurements of the angular correlation function in real space. The bias formally remains finite at all angular scales as a result of mode coupling.

process, adopting a minimal width for the angular binning set by the pixel size. In Fig. 5 we show results at several different values of θ in comparison with the analytical estimate obtained from equation (31), finding good agreement. We note that the data points are significantly correlated across all angular scales.

4.3 Discussion

While the conclusions presented in Section 2 remain qualitatively unchanged, we find that applying template cleaning in real space leads to somewhat different bias estimates. Unfortunately, the coupling of Fourier modes in angular correlation function estimates complicates the analytical bias calculation.

While power spectra are a function of an integer variable ℓ, the argument of the angular correlation function is a real number. It is therefore necessary to adopt some binning scheme for the latter and average the measurements over angular separations in intervals with finite width, $\theta_{\rm min} \leq \theta \leq \theta_{\rm max}$. Since varying the binning will result in a different bias introduced by the cleaning procedure, we consider the use of Monte Carlo simulations to correct angular correlation function estimates cleaned with the template subtraction method to be the preferred strategy in practical applications. For that reason, we limited the derivation of analytical results to a single example.

5 SUMMARY AND CONCLUSIONS

Measurements of the angular clustering of cosmological data have become a standard analysis tool in modern cosmology. To mitigate the impact of systematic effects, capable of introducing spurious signals of non-cosmological origin, a number of approaches have been proposed in literature. Concentrating on three popular techniques, template subtraction (Ho et al. 2012), basic mode projection (Rybicki & Press 1992), and extended mode projection (Leistedt & Peiris 2014), we presented an in-depth discussion of the effects of the systematics mitigation method on the inferred power spectrum estimates. Based on a rigorous mathematical analysis, and in agreement with simulations, we concluded that two out of the three methods – template subtraction and extended mode projection – return biased estimates of the cleaned signal power spectra. In detail, we obtain the following results:

For template subtraction, we derived closed-form expressions for the multipole-dependent bias in the most general case considered here, the cleaning of data with multiple templates on the cut sky. We explained its root cause as a consequence of chance correlations between the signal realization and the template. Our results then allow debiased power spectrum estimates to be obtained with this method, or, equivalently, measurements of the angular correlation function. We further identified an increase in variance of the estimates and concluded that for a given number of cleaning templates, the clustering on specific angular scales can no longer be measured. Extending the discussion to the template cleaning of angular correlation function estimates, we obtained consistent results. Since we found the analytical bias calculation in real space to be more involved, we proposed to mainly use simulations to obtain the correction factor needed to debias results.

The analysis of basic mode projection showed that power spectrum estimates remain unbiased in this framework. We verified analytically that mode projection increases the estimator variance and introduces additional coupling between Fourier modes. Owing to the details of the cleaning process, we found the excess variance to be smaller than for the template subtraction method.

Lastly, assessing the properties of the extended mode projection algorithm, we identified the power spectrum estimates to be biased. Since the basic mode projection algorithm has been proven bias-free, we showed that it results from the selection process that was used to decide if a given template should be marginalized over. We concluded that the bias originates from chance correlations between the template and the data, which introduce an implicit dependence of the selection process on the signal amplitude. Although we were able to obtain analytical expressions that would in principle allow debiased power spectrum estimates, they depend on the details of the adopted template selection criterion as well as on the actual level of contamination, which we presume unknown. We conclude that additional information, for example provided by forward-modelling simulations of the data including systematics, is necessary to obtain unbiased signal estimates.

ACKNOWLEDGEMENTS

We thank our referee, Ashley Ross, for his valuable comments that helped improving the presentation of our results. We are grateful to Hans Kristian Eriksen for useful discussions. FE, BL, and HVP were partially supported by the European Research Council under the European Community's Seventh Framework Programme (FP7/2007-2013) / ERC grant agreement no 306478-CosmicDawn. Some of the results in this paper have been derived using the HEALPIX[2] (Górski et al. 2005) package.

REFERENCES

Benítez N. et al., 2015, in Cenarro A. J., Figueras F., Hernández-Monteagudo C., Trujillo Bueno J., Valdivielso L., eds, Proc. XI Scientific Meeting of the Spanish Astronomical Society. Highlights of Spanish Astrophysics VIII, Teruel, Spain, p. 148
Bergé J., Gamper L., Réfrégier A., Amara A., 2013, Astron. Comput., 1, 23
Beutler F. et al., 2011, MNRAS, 416, 3017
Blake C., Wall J., 2002, MNRAS, 329, L37
Blake C. et al., 2010, MNRAS, 406, 803
Busca N. G. et al., 2013, A&A, 552, A96
Busha M. T., Wechsler R. H., Becker M. R., Erickson B., Evrard A. E., 2013, in AAS Meeting, Vol. 221. Catalog Production for the DES Blind Cosmology Challenge. p. 341.07
Chang C. et al., 2015, ApJ, 801, 73
Cole S. et al., 2005, MNRAS, 362, 505

[2] http://healpix.sourceforge.net

Condon J. J., Cotton W. D., Greisen E. W., Yin Q. F., Perley R. A., Taylor G. B., Broderick J. J., 1998, AJ, 115, 1693
Crocce M. et al., 2015, preprint (arXiv:1507.05360)
de Jong J. T. A., Verdoes Kleijn G. A., Kuijken K. H., Valentijn E. A., 2013, Exp. Astron., 35, 25
Drinkwater M. et al., 2006, Anglo-Aust. Obs. Epping Newsl., 110, 3
Eisenstein D. J. et al., 2005, ApJ, 633, 560
Elsner F., Wandelt B. D., 2013, A&A, 549, A111
Frieman J., Dark Energy Survey Collaboration, 2013, in AAS Meeting, Vol. 221, The Dark Energy Survey: Overview. p. 335.01
Giannantonio T. et al., 2015, preprint (arXiv:1507.05551)
Górski K. M., Hivon E., Banday A. J., Wandelt B. D., Hansen F. K., Reinecke M., Bartelmann M., 2005, ApJ, 622, 759
Hermit S., Santiago B. X., Lahav O., Strauss M. A., Davis M., Dressler A., Huchra J. P., 1996, MNRAS, 283, 709
Hinshaw G. et al., 2007, ApJS, 170, 288
Hivon E., Górski K. M., Netterfield C. B., Crill B. P., Prunet S., Hansen F., 2002, ApJ, 567, 2
Ho S. et al., 2012, ApJ, 761, 14
Huchra J., Davis M., Latham D., Tonry J., 1983, ApJS, 52, 89
Huterer D., Cunha C. E., Fang W., 2013, MNRAS, 432, 2945
Ilbert O. et al., 2006, A&A, 457, 841
Jones D. H. et al., 2004, MNRAS, 355, 747
Kaiser N. et al., 2010, in Stepp L. M., Gilmozzi R., Hall H. J., eds, Proc. SPIE Conf. Ser. Vol. 7733, Ground-based and Airborne Telescopes III. SPIE, Bellingham, p. 77330E
Landy S. D., Szalay A. S., 1993, ApJ, 412, 64
Leistedt B., Peiris H. V., 2014, MNRAS, 444, 2
Leistedt B., Peiris H. V., Mortlock D. J., Benoit-Lévy A., Pontzen A., 2013, MNRAS, 435, 1857
Leistedt B., Peiris H. V., Roth N., 2014, Phys. Rev. Lett., 113, 221301
Leistedt B. et al., 2015, preprint (arXiv:1507.05647)
LSST Dark Energy Science Collaboration, 2012, preprint (arXiv:1211.0310)
McMahon R. G., Banerji M., Gonzalez E., Koposov S. E., Bejar V. J., Lodieu N., Rebolo R., VHS Collaboration, 2013, The Messenger, 154, 35
Morrison C. B., Hildebrandt H., 2015, MNRAS, 454, 3121
Padmanabhan N. et al., 2007, MNRAS, 378, 852
Peebles P. J. E., Hauser M. G., 1974, ApJS, 28, 19
Percival W. J. et al., 2010, MNRAS, 401, 2148
Reid B. A. et al., 2010, MNRAS, 404, 60
Ross A. J. et al., 2011, MNRAS, 417, 1350
Ross A. J. et al., 2012, MNRAS, 424, 564
Rybicki G. B., Press W. H., 1992, ApJ, 398, 169
Saha R., Prunet S., Jain P., Souradeep T., 2008, Phys. Rev. D, 78, 023003
Scranton R. et al., 2002, ApJ, 579, 48
Skrutskie M. F. et al., 2006, AJ, 131, 1163
Slosar A., Seljak U., Makarov A., 2004, Phys. Rev. D, 69, 123003
Smith K. M., Senatore L., Zaldarriaga M., 2009, J. Cosmol. Astropart. Phys., 9, 6
Tegmark M., 1997, Phys. Rev. D, 55, 5895
Tegmark M., Hamilton A. J. S., Strauss M. A., Vogeley M. S., Szalay A. S., 1998, ApJ, 499, 555
Tegmark M. et al., 2004, ApJ, 606, 702
Totsuji H., Kihara T., 1969, PASJ, 21, 221
Vargas-Magaña M. et al., 2014, MNRAS, 445, 2
Wake D. A. et al., 2011, ApJ, 728, 46
York D. G. et al., 2000, AJ, 120, 1579
Zehavi I. et al., 2002, ApJ, 571, 172

APPENDIX A: TEMPLATE SUBTRACTION

A1 full-sky analysis with multiple templates

We now extend our results derived in Section 2 for a single template to an arbitrary number n of linearly independent templates using the updated data model

$$d = s + \sum_{i=1}^{n} \epsilon_i f_i. \tag{A1}$$

To this end, we first have to generalize the estimator equation (2) by transforming it into a matrix equation,

$$\widehat{C}_\ell^{\rm TS} = \widehat{C}_\ell^{d\times d} - \hat{\boldsymbol{\epsilon}}^\dagger \widehat{\boldsymbol{C}}_\ell^{f\times f} \hat{\boldsymbol{\epsilon}}, \tag{A2}$$

where $\hat{\boldsymbol{\epsilon}}^\dagger = (\hat{\epsilon}_1, \ldots, \hat{\epsilon}_n)$, and $\left(\widehat{\boldsymbol{C}}_\ell^{f\times f}\right)_{ij} = \widehat{C}_\ell^{f_i\times f_j}$. Contrary to the single template case, the estimates for $\hat{\boldsymbol{\epsilon}}$ are now computed by solving a system of linear equations,

$$\hat{\boldsymbol{\epsilon}} = \widehat{\boldsymbol{C}}_\ell^{f\times f\,-1} \widehat{\boldsymbol{C}}_\ell^{d\times f}, \tag{A3}$$

where the vectors $\left(\widehat{\boldsymbol{C}}_\ell^{d\times f}\right)_i = \widehat{C}_\ell^{d\times f_i}$. We find,

$$\begin{aligned}\widehat{C}_\ell^{\rm TS} &= \widehat{C}_\ell^{d\times d} - \widehat{\boldsymbol{C}}_\ell^{d\times f\,\dagger} \widehat{\boldsymbol{C}}_\ell^{f\times f\,-1} \widehat{\boldsymbol{C}}_\ell^{d\times f} \\ &= \widehat{C}_\ell^{s\times s} - \widehat{\boldsymbol{C}}_\ell^{s\times f\,\dagger} \widehat{\boldsymbol{C}}_\ell^{f\times f\,-1} \widehat{\boldsymbol{C}}_\ell^{s\times f}.\end{aligned} \tag{A4}$$

To show the equality of the two right-hand side expressions, we first note that, given equation (A1),

$$\widehat{C}_\ell^{d\times d} = \widehat{C}_\ell^{s\times s} + 2\sum_i \hat{\epsilon}_i \widehat{C}_\ell^{s\times f_i} + \sum_{ij} \hat{\epsilon}_i \hat{\epsilon}_j \widehat{C}_\ell^{f_i\times f_j}. \tag{A5}$$

Using $\widehat{C}_\ell^{d\times f_i} = \widehat{C}_\ell^{s\times f_i} + \sum_j \hat{\epsilon}_j \widehat{C}_\ell^{f_i\times f_j}$, we obtain

$$\begin{aligned}\widehat{\boldsymbol{C}}_\ell^{d\times f\,\dagger} \widehat{\boldsymbol{C}}_\ell^{f\times f\,-1} \widehat{\boldsymbol{C}}_\ell^{d\times f} &= \widehat{\boldsymbol{C}}_\ell^{s\times f\,\dagger} \widehat{\boldsymbol{C}}_\ell^{f\times f\,-1} \widehat{\boldsymbol{C}}_\ell^{s\times f} \\ &\quad + 2\sum_{ijq} \left(\widehat{\boldsymbol{C}}_\ell^{f\times f\,-1}\right)_{ij} \widehat{C}_\ell^{f_j\times f_q} \hat{\epsilon}_q \widehat{C}_\ell^{s\times f_i} \\ &\quad + \sum_{ijpq} \left(\widehat{\boldsymbol{C}}_\ell^{f\times f\,-1}\right)_{ij} \widehat{C}_\ell^{f_j\times f_q} \hat{\epsilon}_q \hat{\epsilon}_p \widehat{C}_\ell^{f_i\times f_p},\end{aligned} \tag{A6}$$

from which equation (A4) follows. Applying the same procedure as in equation (6), we find for the ensemble averaged signal power spectrum estimate

$$\begin{aligned}\left\langle \widehat{C}_\ell^{\rm TS} \right\rangle &= C_\ell^{s\times s} - \left\langle \widehat{\boldsymbol{C}}_\ell^{s\times f\,\dagger} \widehat{\boldsymbol{C}}_\ell^{f\times f\,-1} \widehat{\boldsymbol{C}}_\ell^{s\times f} \right\rangle \\ &= C_\ell^{s\times s} - \frac{C_\ell^{s\times s}}{2\ell+1} \sum_{ij} \left(\boldsymbol{C}_\ell^{f\times f\,-1}\right)_{ij} C_\ell^{f_i\times f_j} \\ &= C_\ell^{s\times s} \left(1 - \frac{n}{2\ell+1}\right),\end{aligned} \tag{A7}$$

i.e. the generalized expression for the relative bias on the full sky is $b_\ell = -n/(2\ell+1)$.

A2 Cut-sky analysis with a single template

For completeness, we start by listing the definitions of the pseudo-C_ℓ coupling kernels and matrices used in Section 2.2, as derived by Hivon et al. (2002). Setting $a_{\ell m}[][][a]$ to be the spherical harmonic expansion coefficients of an unmasked map on the full sky, the effect of an arbitrary real window function W then results in a related set of coefficients $a_{\ell m}$,

$$\begin{aligned}a_{\ell m} &= \sum_{\ell' m'} \bar{a}_{\ell' m'} \int {\rm d}\boldsymbol{n} Y_{\ell' m'} W(\boldsymbol{n}) Y^*_{\ell m} \\ &= \sum_{\ell' m'} \bar{a}_{\ell' m'} K_{\ell m \ell' m'}.\end{aligned} \tag{A8}$$

The coupling kernels K can be explicitly expressed in terms of a product of Gaunt coefficient with $W_{\ell m}$, the spherical harmonic expansion of the mask,

$$K_{\ell_1 m_1 \ell_2 m_2} = \sum_{\ell_3 m_3} w_{\ell_3 m_3} (-1)^{m_2} \times \left[\frac{(2\ell_1+1)(2\ell_2+1)(2\ell_3+1)}{4\pi}\right]^{1/2} \times \begin{pmatrix} \ell_1 & \ell_2 & \ell_3 \\ 0 & 0 & 0 \end{pmatrix} \begin{pmatrix} \ell_1 & \ell_2 & \ell_3 \\ m_1 & -m_2 & m_3 \end{pmatrix}, \tag{A9}$$

where the last two factors are Wigner 3j symbols.

The pseudo-C_ℓ coupling matrices then relate the power spectrum of the masked coefficients $a_{\ell m}$to the full-sky coefficients $\bar{a}_{\ell m}$ such that the pseudo-C_ℓ estimates become unbiased, $\left\langle \widehat{C}_\ell \right\rangle = \sum_{\ell'} M_{\ell\ell'} \left\langle \widehat{C}^{\rm PCL}_{\ell'} \right\rangle = C_\ell$. Given the orthogonality relations of the Wigner 3j symbols, they take a particularly simple form,

$$M_{\ell_1\ell_2} = \frac{2\ell_2+1}{4\pi} \sum_{\ell_3} (2\ell_3+1) C^{w\times w}_{\ell_3} \begin{pmatrix} \ell_1 & \ell_2 & \ell_3 \\ 0 & 0 & 0 \end{pmatrix}^2. \tag{A10}$$

With the definitions given above, we can now derive the result quoted in equation (9). For brevity, let $X = \langle (\widehat{C}_\ell^{s\times f})^2 \rangle$, then

$$\begin{aligned} X = & \sum_{\substack{\ell_1 m_1 \\ \ell_2 m_2}} M^{-1}_{\ell\ell_1} M^{-1}_{\ell\ell_2} \frac{1}{2\ell_1+1} \frac{1}{2\ell_2+1} \\ & \times \sum_{\ell_3 m_3} C^{s\times s}_{\ell_3} K_{\ell_1 m_1 \ell_3 m_3} K^*_{\ell_2 m_2 \ell_3 m_3} \\ & \times \sum_{\ell_4 m_4} C^{f\times f}_{\ell_4} K^*_{\ell_1 m_1 \ell_4 m_4} K_{\ell_2 m_2 \ell_4 m_4}. \end{aligned} \tag{A11}$$

Expanding the coupling kernels using equation (A9), we obtain

$$\begin{aligned} X = & \sum_{\substack{\ell_1 m_1 \\ \ell_2 m_2}} M^{-1}_{\ell\ell_1} M^{-1}_{\ell\ell_2} \frac{1}{2\ell_1+1} \frac{1}{2\ell_2+1} \\ & \times \sum_{\substack{\ell_3 m_3 \\ \ell_4 m_4}} C^{s\times s}_{\ell_3} C^{w\times w}_{\ell_4} (-1)^{m_2+m_3+m_4} \sqrt{(2\ell_1+1)(2\ell_2+1)} \\ & \times \frac{(2\ell_3+1)(2\ell_4+1)}{4\pi} \begin{pmatrix} \ell_1 & \ell_3 & \ell_4 \\ 0 & 0 & 0 \end{pmatrix} \begin{pmatrix} \ell_2 & \ell_3 & \ell_4 \\ 0 & 0 & 0 \end{pmatrix} \\ & \times \begin{pmatrix} \ell_1 & \ell_3 & \ell_4 \\ m_1 & -m_3 & m_4 \end{pmatrix} \begin{pmatrix} \ell_2 & \ell_3 & \ell_4 \\ -m_2 & m_3 & -m_4 \end{pmatrix} \\ & \times \sum_{\substack{\ell_5 m_5 \\ \ell_6 m_6}} C^{f\times f}_{\ell_5} C^{w\times w}_{\ell_6} (-1)^{m_1+m_5+m_6} \sqrt{(2\ell_1+1)(2\ell_2+1)} \\ & \times \frac{(2\ell_5+1)(2\ell_6+1)}{4\pi} \begin{pmatrix} \ell_1 & \ell_5 & \ell_6 \\ 0 & 0 & 0 \end{pmatrix} \begin{pmatrix} \ell_2 & \ell_5 & \ell_6 \\ 0 & 0 & 0 \end{pmatrix} \\ & \times \begin{pmatrix} \ell_1 & \ell_5 & \ell_6 \\ -m_1 & m_5 & -m_6 \end{pmatrix} \begin{pmatrix} \ell_2 & \ell_5 & \ell_6 \\ m_2 & -m_5 & m_6 \end{pmatrix}. \end{aligned} \tag{A12}$$

By first performing the sum over the projective quantum numbers m_3, m_4, m_5, and m_6, combined with the orthogonality relations of the Wigner 3j symbols and upon substituting equation (A8), we arrive at the much simplified expression equation (9).

APPENDIX B: BASIC MODE PROJECTION

B1 Estimator mean and variance

Here, we prove the identities used in the derivation of equations (19), (20), and (21). To do so, we first obtain simplified expressions for a series of terms we will make use of in the process. We find

$$\mathrm{tr}\left(\boldsymbol{D}_\ell f f^\dagger\right) = (2\ell+1) C^{f\times f}_\ell, \tag{B1}$$

$$f^\dagger \widetilde{\boldsymbol{C}}^{-1} f = \sum_\ell (2\ell+1) \frac{C^{f\times f}_\ell}{C^{s\times s}_\ell}, \tag{B2}$$

$$\begin{aligned} & \mathrm{tr}\left(\widetilde{\boldsymbol{C}}^{-1} f f^\dagger \boldsymbol{D}_\ell \widetilde{\boldsymbol{C}}^{-1} f f^\dagger\right) \\ & \quad = (2\ell+1) \frac{C^{f\times f}_\ell}{C^{s\times s}_\ell} \sum_{\ell'} (2\ell'+1) \frac{C^{f\times f}_{\ell'}}{C^{s\times s}_{\ell'}}, \end{aligned} \tag{B3}$$

$$\mathrm{tr}\left(\widetilde{\boldsymbol{C}}^{-1} f f^\dagger \boldsymbol{D}_\ell \widetilde{\boldsymbol{C}}^{-1} f f^\dagger \boldsymbol{D}_\ell\right) = \left[(2\ell+1)\frac{C^{f\times f}_\ell}{C^{s\times s}_\ell}\right]^2. \tag{B4}$$

Then, from

$$\begin{aligned} \left\langle \boldsymbol{d}^\dagger \widetilde{\boldsymbol{E}}_\ell \boldsymbol{d} \right\rangle = & \frac{1}{C^{s\times s}_\ell} \\ & \times \mathrm{tr}\left[\left(\boldsymbol{D}_\ell - \frac{\boldsymbol{C}^{-1} f f^\dagger \boldsymbol{D}_\ell}{f^\dagger \boldsymbol{C}^{-1} f}\right)\left(1 - \frac{\boldsymbol{C}^{-1} f f^\dagger}{f^\dagger \boldsymbol{C}^{-1} f}\right)\right], \end{aligned} \tag{B5}$$

equation (19) follows. Likewise, we find for

$$\begin{aligned} \widetilde{N}_{\ell\ell} = & \frac{1}{\left(C^{s\times s}_\ell\right)^2} \\ & \times \mathrm{tr}\left[\left(\boldsymbol{D}_\ell - \frac{\boldsymbol{C}^{-1} f f^\dagger \boldsymbol{D}_\ell}{f^\dagger \boldsymbol{C}^{-1} f}\right)\left(\boldsymbol{D}_\ell - \frac{\boldsymbol{C}^{-1} f f^\dagger \boldsymbol{D}_\ell}{f^\dagger \boldsymbol{C}^{-1} f}\right)\right], \end{aligned} \tag{B6}$$

and

$$\widetilde{N}_{\ell\ell'} = \frac{1}{C^{s\times s}_\ell C^{s\times s}_{\ell'}} \mathrm{tr}\left(\frac{\boldsymbol{C}^{-1} f f^\dagger \boldsymbol{D}_\ell \boldsymbol{C}^{-1} f f^\dagger \boldsymbol{D}_{\ell'}}{\left(f^\dagger \boldsymbol{C}^{-1} f\right)^2}\right) \tag{B7}$$

for $\ell \neq \ell'$, and therefore obtain equations (20) and (21).

B2 Proof of unbiasedness

Given our results summarized in equations (19), (20), and (21), we now want to show that the quadratic estimator remains unbiased when mode projection is included, i.e. $\sum_{\ell'} \widetilde{N}^{-1}_{\ell\ell'} \langle \boldsymbol{d}^\dagger \widetilde{\boldsymbol{E}}_{\ell'} \boldsymbol{d} \rangle = C^{s\times s}_\ell$. As it turns out, it is simpler to prove the equivalent expression $\langle \boldsymbol{d}^\dagger \widetilde{\boldsymbol{E}}_\ell \boldsymbol{d} \rangle = \sum_{\ell'} \widetilde{N}_{\ell\ell'} C^{s\times s}_{\ell'}$ instead. Indeed, we find,

$$\begin{aligned} \sum_{\ell'} \widetilde{N}_{\ell\ell'} C^{s\times s}_{\ell'} = & \frac{2\ell+1}{C^{s\times s}_\ell} \left(1 - 2\frac{C^{f\times f}_\ell / C^{s\times s}_\ell}{\sum_{\ell'} (2\ell'+1) C^{f\times f}_{\ell'} / C^{s\times s}_{\ell'}} \right. \\ & + \frac{C^{f\times f}_\ell / C^{s\times s}_\ell}{\sum_{\ell'} (2\ell'+1) C^{f\times f}_{\ell'} / C^{s\times s}_{\ell'}} \\ & \left. \times \sum_{\ell'} \frac{(2\ell'+1) C^{f\times f}_{\ell'} / C^{s\times s}_{\ell'}}{\sum_{\ell''} (2\ell''+1) C^{f\times f}_{\ell''} / C^{s\times s}_{\ell''}} \right) \\ = & \left\langle \boldsymbol{d}^\dagger \widetilde{\boldsymbol{E}}_\ell \boldsymbol{d} \right\rangle. \end{aligned} \tag{B8}$$

This paper has been typeset from a TEX/LATEX file prepared by the author.